ACS APPLIED MATERIALS & INTERFACES

Research Article

www.acsami.org

First-Principles Prediction of New Photocatalyst Materials with Visible-Light Absorption and Improved Charge Separation: Surface Modification of Rutile TiO_2 with Nanoclusters of MgO and Ga_2O_3

Michael Nolan*

Tyndall National Institute, University College Cork, Lee Maltings, Prospect Row, Cork, Ireland

ABSTRACT: Titanium dioxide is an important and widely studied photocatalytic material, but to achieve photocatalytic activity under visible-light absorption, it needs to have a narrower band gap and reduced charge carrier recombination. First-principles simulations are presented in this paper to show that heterostructures of rutile TiO_2 modified with nanoclusters of MgO and Ga_2O_3 will be new photocatalytically active materials in the UV (MgO-TiO_2) and visible (Ga_2O_3–TiO_2) regions of the solar spectrum. In particular, our investigations of a model of the excited state of the heterostructures demonstrate that upon light excitation electrons and holes can be separated onto the TiO_2 surface and the metal oxide nanocluster, which will reduce charge recombination and improve photocatalytic activity. For MgO-modified TiO_2, no significant band gap change is predicted, but for Ga_2O_3-modified TiO_2, we predict a band gap change of up to 0.6 eV, which is sufficient to induce visible light absorption. Comparisons with unmodified TiO_2 and other TiO_2-based photocatalyst structures are presented.

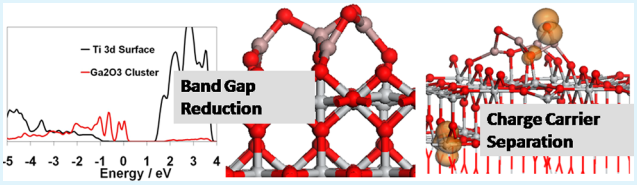

KEYWORDS: *photocatalyst, TiO_2, DFT+U, visible-light absorption, surface modification, charge separation*

1. INTRODUCTION

Photocatalysts based on metal oxides have the potential to be low-cost, environmentally friendly, earth-abundant solutions for solar hydrogen production from water splitting,[1−3] CO_2 reduction to hydrocarbons,[4,5] and environmental depollution by destruction of organic pollutants[6,7] The leading material in this regard is titanium dioxide, TiO_2, which is cheap, readily available, and nontoxic. Because the band gap of rutile and anatase lies in the UV region (3−3.2 eV, depending on crystal form), a major issue in delivering future photocatalytic technologies is to engineer the light absorption properties of TiO_2 so that it has a band gap in the visible region of the solar spectrum, thus using a larger fraction of the available solar energy than that available in the UV.[8] In these efforts, first-principles density functional theory (DFT) simulations are being extensively used in conjunction with experiment.

Generally, efforts in modifying TiO_2 to enhance visible-light absorption have focused on substitution of metal cations and/or non-metal anions at Ti and O sites in rutile or anatase.[9−17] In some cases, DFT calculations show that this modification can potentially reduce the band gap into the visible, although the choice of DFT methodology can impact on these findings.[17] Some experimental results on, e.g. N-doped TiO_2, indicate visible light absorption.[18−21] Recently, there has been work on so-called co-doping with compensating cation−anion pairs[22,23] from DFT simulations, with a recent experimental study of Mo−C co-doped TiO_2.[24] Although the aim of narrowing the band gap has been an important activity, it has to be emphasised that other issues like stability, solubility, and reproducibility in the area of TiO_2 doping are also important and the question of how doping impacts on charge recombination and ultimately on photocatalytic activity, even with band gap reduction, must be considered. This has generally been lacking in DFT simulations, which have focused almost exclusively on band gap reduction because of doping, and neglected effects on charge recombination.

An alternative approach, which should be more robust than substitutional doping, is to exploit structural engineering of nanostructures and interfaces in TiO_2. For example, there has been great interest in synthesizing anatase TiO_2 structures with (001) surface exposed, rather than the more stable (101) surface. The (001) anatase surface is more photocatalytically active than the (101) surface.[25−29] Nanostructuring is another route to band gap and charge transport engineering, with nanostructures showing structure-dependent band gaps and providing short charge diffusion pathways that reduce recombination.[26−30] A very exciting approach is to fabricate heterostructures, which are composed of two different metal oxides or two different structures interfaced together, with the interface playing a key role.[31−44] Recent results indicate that this heterostructuring approach is a successful and versatile approach to tune the structure to give visible light absorption and improved photocatalytic activity.[31−44] Oxide-oxide structures such as BiOBr−$ZnFe_2O_4$,[32] AgI−BiO,[33] $BiVO_4$−WO_3,[34] $Bi_4Ti_3O_{12}$−TiO_2[35] and SnO_x−$ZnGa_2O_4$,[36] and their interfaces display a band gap reduction, shifting the photoactivity into the visible region and promoting electron/hole separation, to reduce recombination, giving improved photocatalytic activity over the pure oxides.

Received: August 1, 2012
Accepted: October 12, 2012
Published: October 12, 2012

   dx.doi.org/10.1021/am301516c | *ACS Appl. Mater. Interfaces* 2012, 4, 5863−5871

Combining the ideas of heterostructure formation and nanostructuring, Libera et al.[37] and Tada et al.[38−42] fabricated TiO_2 surface modified with transition metal oxide nanoclusters. Libera et al. deposited Fe_2O_3 nanoclusters by atomic layer deposition (ALD) on TiO_2,[37] whereas Tada et al. synthesised (FeO_x)-modified TiO_2 using the chemisorption-calcination (CCC) technique to deposit highly dispersed FeO_x nanoclusters on TiO_2 surface at a molecular scale.[38,39] Both groups found greatly improved visible-light activity and no impact on UV-light activity, which is postulated to arise from band gap narrowing because of the presence of the FeO_x clusters shifting the top of the TiO_2 valence band.[37,38] Photoluminescence spectroscopy showed a decrease in electron-hole recombination,[38] characterised by a suppression in the well-known PL peak of TiO_2 at 540 nm in the FeO_x-modified TiO_2 structures. Subsequently, NiO[40] and SnO_2[41,42] nanoclusters have been studied as further examples of surface-modified TiO_2 photocatalysts, with improved photoactivity and reduced charge recombination. Recent work has shown that the chemical state of the metal oxide deposited on TiO_2, as well as the TiO_2 crystal form, is important.[36,41,42] For example, the non-transition-metal SnO_2 modification leads to a small enhancement of visible-light activity and an enhancement of UV activity for rutile modified TiO_2, but only UV activity for anatase modified with SnO_2.[41,42] On $ZnGa_2O_4$, SnO_2 modification results in no visible-light activity, but modification with SnO results in visible-light absorption.[36] This demonstrates that the chemical state of the metal oxide nanoclusters plays a role.

While these structures show extremely good promise as novel photocatalysts, further work is needed to understand their fundamental properties and allow the development of surface-modified TiO_2 as new photocatalyst materials.

To illuminate the experimental studies, density functional theory (DFT) simulations of TiO_2-modified with small metal oxide clusters[43−45] have confirmed the origin of the band gap reduction in FeO_x-modified rutile TiO_2[43] and the origin of enhanced UV- or visible-light activity of SnO_2-modified anatase[41,42] or rutile[44] TiO_2. We have also shown that sub-nanometer diameter $(TiO_2)_n$ clusters and CrO_x and Mo_2O_4 deposited on the rutile TiO_2 (110) surface will lead to a reduced band gap compared to pure rutile TiO_2. In addition, the energy level alignments in the heterostructures are suggested to facilitate charge separation, thus enhancing photocatalytic activity.[45] Thus, DFT simulations provide an invaluable tool to design and understand modified novel TiO_2-based materials for photocatalysis.

In further developing and understanding surface-modified TiO_2, photocatalysts, this paper presents a first-principles DFT prediction of new visible and UV-active photocatalysts that are composed of rutile TiO_2 (110) modified with non-transition-metal oxide nanoclusters, namely MgO and Ga_2O_3. Visible-light photocatalytic activity is predicted in Ga_2O_3-modified TiO_2 through band gap reduction, with enhanced UV activity predicted for MgO-modified TiO_2. Although there is no previous work in the literature on Ga_2O_3-modified TiO_2, there have been some studies of MgO.[46−50] In ref 46., Shao et al. coated mesoporous TiO_2 with MgO by evaporation induced self-assembly (EISA) combined with impregnation, with improved UV-photocatalytic activity. Bandara et al.[47,48] also coated TiO_2 with MgO and found higher dye degradation over bare TiO_2, which was attributed to the retardation of charge recombination in the composite. Jung et al.[49] prepared TiO_2−MgO core−shell nanoparticles that showed improved photocatalytic activity over bare TiO_2. Finally, Tada et al.[50] have prepared TiO_2 modified with sub-monolayer MgO showing enhanced activity for photocatalytic degradation of dodecylbenzenesulfonate.

To study the charge carrier separation, which is important for photocatalytic activity, in both heterostructures, we use a model of the photoexcited[51,52] electronic state to show for the first time that the electronic structure of surface-modified TiO_2 promotes charge carrier (electron and hole) separation and we identify the electron and hole trapping sites in the TiO_2 surface and the metal oxide nanocluster, confirming the expectation regarding charge carrier separation. We therefore show (1) the origin of the enhanced activity of MgO-modified TiO_2 and (2) the prediction of Ga_2O_3-modified TiO_2 as photocatalysts with improved activity over unmodified TiO_2.

2. METHODOLOGY

To model the TiO_2 rutile (110) surface, we use a three dimensional periodic slab model and a plane wave basis set to describe the valence electronic wave functions within the VASP code.[53] The cut-off for the kinetic energy is 396 eV. For the core−valence interaction we apply Blöchl's projector augmented wave (PAW) method,[54] with Ti described by 4 valence electrons and oxygen by 6 valence electrons; Mg is described with 2 valence electrons, and Ga with 3 valence electrons. We use the Perdew−Wang91 approximation to the exchange-correlation functional.[55] k-point sampling is performed using the Monkhorst-Pack scheme, with a $(2 \times 2 \times 1)$ sampling grid.

For describing the electronic states of Ti in TiO_2, we have used the DFT+U approach. DFT+U[56,57] adds a Hubbard U correction to describe reduced metal cation states, such as Ti^{3+} polarons, that are found in photoexcited TiO_2. From the literature, values of U in the range 3−5 eV are reasonable,[43−45,58−60] and we apply $U = 4.5$ eV to the Ti 3d states throughout this paper. For Mg and Ga, no +U correction is required, since the electronic states are reasonably well-described with DFT. Although DFT+U can treat some of the problems with DFT in describing partially filled electronic states, it is an approximate method and still does not fully deal with the band gap underestimation in approximate DFT and the energy gaps resulting from this work will be underestimated and can show some dependence on the precise DFT+U setup. Calculations using hybrid DFT, such as the HSE06 screened exchange method, or time-dependent DFT are more accurate for predicting energy gaps and electronic transitions. However, they are too costly for the structures considered in this paper and cannot be used. However, our DFT+U calculations use robust parameters from the author's own work and the literature[43−45,58−60] and we are primarily interested in qualitative changes in the energy gap resulting from modifications of TiO_2 with metal oxide nanoclusters.

The bulk lattice constants of rutile TiO_2 have been computed by fitting a set of constant volume DFT+U energies to a Murnaghan equation of state, giving the following bulk lattice constants: $a = b = 4.638$ Å, $c = 2.973$ Å. The rutile (110) surface is constructed from this bulk and its structure is well known, with surface terminating two coordinated oxygen (bridging oxygen), surface 5-fold coordinated Ti, surface 6-fold coordinated Ti bound to the bridging oxygen and four fold coordinated in-plane oxygen atoms. A (2×4) surface supercell is employed; this surface supercell expansion is large enough to allow for adsorption of essentially isolated clusters and has been used in many studies of the rutile (110) surface. The rutile surface slab is 6 O−Ti−O layers thick, with a vacuum gap of 10 Å. The bottom trilayer is held fixed and all other layers are allowed relax. The convergence in the wavefunction relaxation is 0.0001 eV, whereas the ionic relaxation is converged when the forces on the atoms are less than 0.02 eV/Å. Fermi level smearing with the Methfessel Paxton scheme is applied, with $\sigma = 0.1$ eV. All calculations are spin polarised.

The metal oxide clusters adsorbed at TiO_2, the bare TiO_2 surface and the free metal oxide clusters are calculated in the same periodic supercell, with the same plane wave cut off energy, the same k-point sampling grid and the same PAW potentials, ensuring consistency between calculations. To study cluster adsorption, the MgO and Ga_2O_3 clusters

are positioned in a number of configurations at the surface and a full relaxation is performed within a fixed supercell. Some short ab initio molecular dynamics simulations in the NVE ensemble with a 0.1 fs timestep at 600 K have been run for 2 ps, with no change in the adsorption structure. The adsorption energy is computed from

$$E_{ads} = E((MO_x) - TiO_2) - \{E(MO_x) + E(TiO_2)\} \quad (1)$$

Where $E((MO_x) - TiO_2)$ is the total energy of the MO_x cluster (M = Mg, Ga) supported on the TiO_2 surface, and $E(MO_x)$ and $E(TiO_2)$ are the total energies of the free MO_x cluster and the bare surface; a negative adsorption energy signifies that cluster adsorption is stable.

In the DOS plots, a smearing of 0.1 eV is used and the cluster DOS are scaled by a factor of 10 to allow for the fact that the cluster contains a maximum 4 cations and 4 anions (MgO) or 4 cations and 6 anions (Ga_2O_3), compared to 96 surface cations and 192 surface anions in rutile (110) to prevent the surface DOS swamping the cluster DOS if the scaling were not otherwise applied.

3. RESULTS

3.1. Structure of MgO and Ga_2O_3-Modified TiO_2. Figure 1 shows the atomic structure of the rutile (110) surface modified by

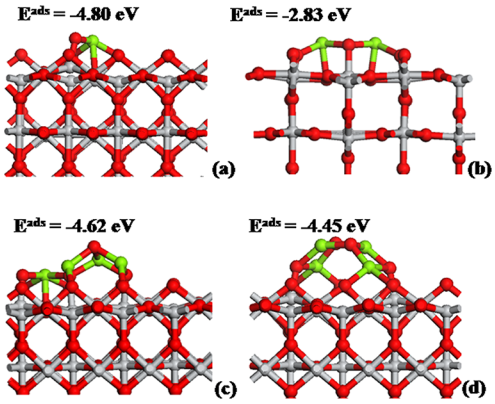

Figure 1. Atomic structure and adsorption energies of the rutile TiO_2 (110) surface modified with MgO nanoclusters. (a) MgO-modified TiO_2; (b) $(MgO)_2$-modified TiO_2; and (c) $(MgO)_4$-modified TiO_2, Structure I; (d) $(MgO)_4$-modified TiO_2, Structure II. Ti is colored grey, Mg is green, and oxygen is red.

adsorption of MgO clusters: MgO, $(MgO)_2$, and $(MgO)_4$. Figure 2 shows the structure of Ga_2O_3 clusters: Ga_2O_3 and $(Ga_2O_3)_2$ adsorbed at the rutile (110) surface. In refs 61 and 62, MgO and Ga_2O_3 clusters were studied using DFT simulations and experiments (the latter in ref 61), and display some non-bulk like low energy cluster structures. Although we have started with free clusters using minimum energy structures presented in these references, the formation of interfacial cluster-surface bonds can modify the metal oxide nanocluster structure quite substantially. For example, although the most stable gas phase $(MgO)_4$ cluster is a cube, the adsorption structure at the rutile (110) surface is more open, which allows for the formation of more metal−oxygen interfacial bonds and strengthens the interaction of the cluster with the surface.

The adsorption energies are also shown in Figures 1 and 2 and indicate that Ga_2O_3 and MgO clusters adsorb strongly at the rutile (110) surface, with the exact energy gain dependent on the cluster size. For MgO, we show as an example of possible adsorption structures two particularly stable structures for the $(MgO)_4$ cluster, which have similar adsorption energies but different structures, indicating that there can be more than one stable adsorption structure with similar adsorption energies. In any case, the clusters will be anchored at the surface, with a

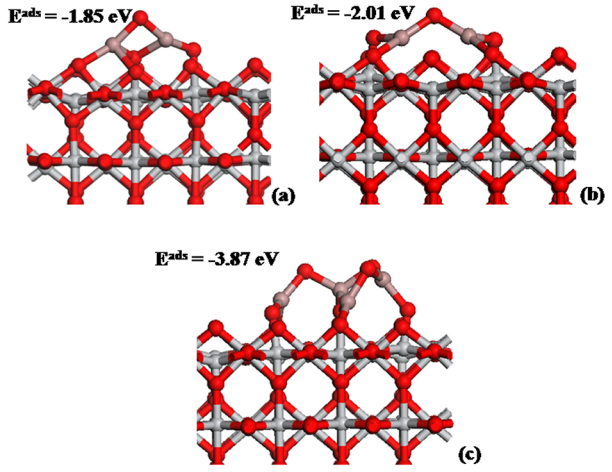

Figure 2. Atomic structure and adsorption energies of the rutile TiO_2 (110) surface modified with Ga_2O_3 clusters. (a) Ga_2O_3-modified TiO_2, structure I; (b) Ga_2O_3-modified TiO_2, structure II; and (c) $(Ga_2O_3)_2$-modified TiO_2. Ti is colored grey, Ga is purple, and oxygen is red.

number of new interfacial metal-oxide bonds formed: e.g. in the most stable $(MgO)_4$ cluster, there are 8 new cluster-surface bonds and in the most stable $(Ga_2O_3)_2$ adsorption structure 6 new cluster-surface bonds are formed. Important metal−oxygen distances between the nanoclusters and the surface are given in table 1.

For MgO clusters adsorbed at the rutile (110) surface, in addition to oxygen from MgO, the Mg atom tends to bind to bridging and in-plane surface oxygen atoms. For the most stable $(MgO)_2$ cluster, the cluster−surface bonding is similar to that found for $(FeO)_2$ nanocluster modified TiO_2.[43] Although the exact metal−oxygen distances depend on the cluster size, in general the distances for cluster Mg to bridging oxygen of the TiO_2 surface tend to be close to the bulk Mg−O distance of 2.10 Å. The Mg−O distances in the cluster will depend on the coordination of the cluster oxygen, but these distances are shorter than in bulk Mg−O, which we also see in the gas phase MgO clusters. Surface Ti to cluster oxygen distances depend strongly on the coordination of the cluster oxygen, which is seen most obviously in the $(MgO)_4$ cluster: here the Ti−O distance to a terminal (singly coordinated) cluster oxygen atom is only 1.79 Å, with the Ti−O distance to a three-fold coordinated cluster oxygen being 2.07 Å. Finally, the surface Ti−O distances involving bridging oxygen are strongly affected by the bonding of these oxygen to Mg in the nanoclusters: the longer Ti−O distance is found when the bridging oxygen has formed a bond to cluster Mg.

For Ga_2O_3 nanocluster adsorption, similar trends are found. For example, the different Ti−O distances for bridging oxygen are also found for Ga_2O_3 nanocluster, although the exact Ti−O distances are longer when compared with adsorbed MgO nanoclusters. Ga−O distances in the adsorbed cluster are shorter than the Ga−O distances in the bulk. In adsorbed Ga_2O_3, the Ga atom binds to two bridging oxygen atoms and an in-plane oxygen in the surface, as well as with oxygen from Ga_2O_3, similar to Fe_2O_3.[43] For the most stable $(Ga_2O_3)_2$ cluster, cluster Ga atoms bind to bridging and in-plane oxygen from the surface.

3.2. Electronic Properties of MgO and Ga_2O_3 Surface-Modified TiO_2. Figure 3 shows the Ti 3d and Mg 3s+3p (figure 3 (a), (b)) and the surface and cluster O 2p (figure 3 (c) and (d)) projected electronic density of states (PEDOS) for TiO_2

dx.doi.org/10.1021/am301516c | ACS Appl. Mater. Interfaces 2012, 4, 5863−5871

Table 1. Selected Mg−O, Ga−O, and Ti−O Distances (in Å) for the Most Stable Adsorption Structures of the MgO- TiO_2 and Ga_2O_3−TiO_2 Heterostructures[a]

Mg^c−O^s	Mg^c−O^c	Ti^s−O^c	Ti^s−O^s
		MgO	
1.97/2.03 (to O^{br})	1.94	1.79	1.88 (to O^{br} not coordinated to Mg)
2.21 (to O^{ip})			1.97/1.98 (to O^{br} coordinated to Mg)
		$(MgO)_2$	
2.15 (× 3 per Mg)	2.04 (× 2 per Mg)	1.85 (× 2)	1.97 (to O^{br} coordinated to Mg)
		$(MgO)_4$ Structure I	
1.91/1.97 (to O^{br})	1.90/1.93/1.97	2.07/1.90/1.79	1.89/1.93 (to O^{br} not coordinated to Mg)
2.09/2.15 (to O^{br})	2.00/2.01/2.09		1.96/1.98 (to O^{br} coordinated to Mg)
2.15 (to O^{ip})			
Ga^c−O^s	Ga^c−O^c	Ti^s−O^c	Ti^s−O^s
		Ga_2O_3 Structure I	
2.07/2.03 (to O^{br})	1.88/1.90	1.82/1.85	1.98/1.99 (to O^{br} not coordinated to Ga)
	1.91/1.95		2.05/2.07 (to O^{br} coordinated to Ga)
		$(Ga_2O_3)_2$	
1.93/1.88/1.98/1.89 (to O^{br})	1.84/1.85/1.86/	1.90/2.07/1.83	1.96/1.97 (to O^{br} not coordinated to Ga)
	1.90/2.16		1.99/205/2.07 (to O^{br} coordinated to Ga)

[a] Mg^c, Ga^c, and O^c signify Mg, Ga, and O from the adsorbed nanocluster, whereas Ti^s and O^s signify Ti and O from the surface. O^{br} and O^{ip} are bridging oxygen and in-plane oxygen from the TiO_2 surface.

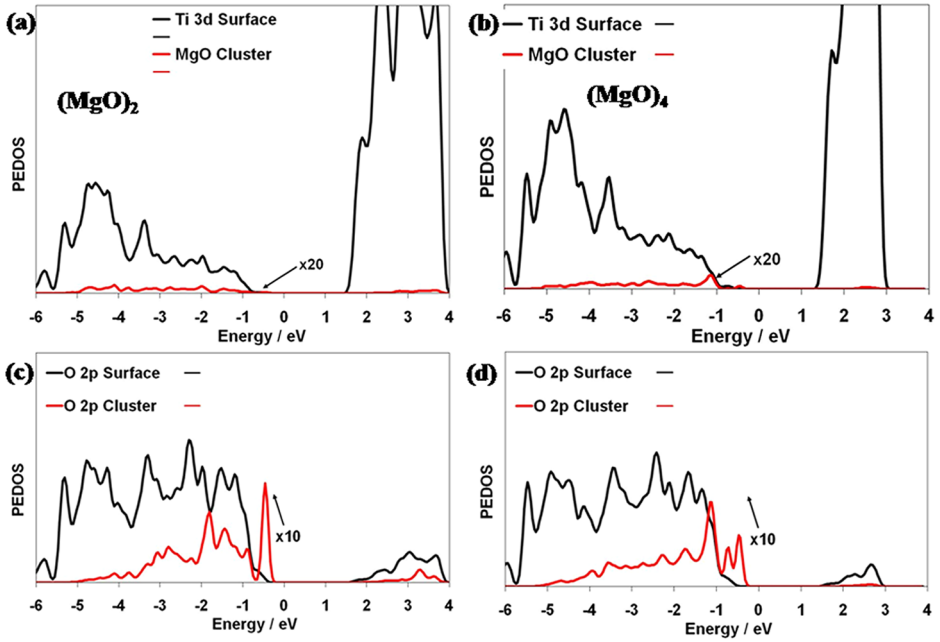

Figure 3. (a) Ti 3d and Mg 3s+3p PEDOS and (c) TiO_2 and MgO O 2p PEDOS for $(MgO)_2$-modified TiO_2. (b) Ti 3d and Mg 3s+3p PEDOS and (d) TiO_2 and MgO O2p PEDOS for $(MgO)_4$-modified TiO_2.

modified with $(MgO)_2$ and $(MgO)_4$ nanoclusters. Examination of the PEODS shows that modification of rutile (110) with MgO does not introduce new states into the band gap of TiO_2. Adsorption of $(MgO)_2$ leads to formation of cluster O2p states at the VB edge of the TiO_2 surface, as indicated by the MgO derived peak in figure 3(c). There are empty Mg-derived states above the conduction band edge of TiO_2. For $(MgO)_4$ adsorbed at TiO_2, there are O 2p derived cluster states around 0.1 eV above the top of the VB. We predict that MgO modification of TiO_2will lead to a small, if any, change to the band gap of TiO_2, with no shift in light absorption to the visible part of the solar spectrum. However, similar to SnO_2 modified anatase,[41] the modifications to the electronic structure induced by the MgO cluster adsorption will lead to an improvement in UV photocatalytic activity. This is important, since UV active photocatalysts are widely used and are still of great importance, despite the recent attention focused on visible light absorption. Improvements in the UV photoactivity of TiO_2 are not to be neglected. The enhanced UV activity is postulated from the enhanced density of states at the VB edge[43] and the presence of empty MgO states above the CB, which will facilitate two aspects: (1) greater absorption of UV light and (2) unoccupied cluster states above the surface CB, into which UV electrons can be excited and from which electrons can be transferred into the TiO_2 conduction band. This energy band structure will drive separation of electrons and holes, thus increasing the UV activity, since electron-hole recombination will be reduced and we will return to this point in section 3.3.

Figure 4 shows the Ti 3d and Ga 4s+4p PEDOS (figure 4 (a), (b)) and the surface and cluster O 2p PEDOS (figure 4 (c), (d))

dx.doi.org/10.1021/am301516c | ACS Appl. Mater. Interfaces 2012, 4, 5863−5871

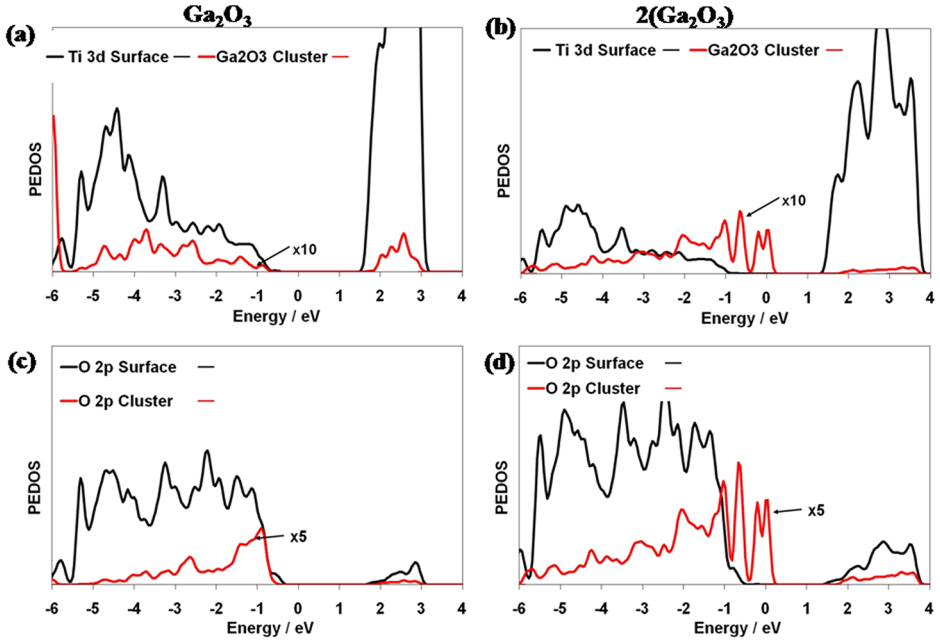

Figure 4. (a) Ti 3d and Ga 4s+4p PEDOS and (c) TiO_2 and Ga_2O_3 O2p PEDOS for Ga_2O_3-modified TiO_2. (b) Ti 3d and Ga 4s+4p PEDOS and (d) TiO_2 and Ga_2O_3 O2p PEDOS for $(Ga_2O_3)_2$-modified TiO_2.

for the Ga_2O_3 cluster modified rutile TiO_2 (110) surface. For both Ga_2O_3 modified TiO_2 heterostructures, we find a different behaviour compared with MgO modified TiO_2. For the smaller cluster, there are Ga_2O_3 O2p states lying at the TiO_2 derived VB edge, with empty Ga_2O_3 states above the TiO_2 conduction band edge. On the other hand, for the larger cluster, there is a clear Ga_2O_3 derived state in the TiO_2 energy gap, offset by around 0.6 eV from the TiO_2 VB edge. The Ga_2O_3 unoccupied states lie above the TiO_2 CB. Therefore, with the Ga_2O_3 cluster modification of rutile TiO_2, we propose that the band gap can be reduced by a sufficient amount to facilitate visible light absorption, while the alignments of the surface and nanocluster energy bands will facilitate charge separation

Modification of TiO_2 with transition metal and non-transition metal oxide nanoclusters has shown that transition metal oxides result in band gap reduction and charge separation.[37−45] But with non-transition metal oxides the effect of the surface modification depends on the identity of the metal oxide involved,[37−45] and this was also observed in experiments on modified ZnGa2O4.[36] The present results and those of ref.,[45] lead us to conclude that a suitable metal oxide with which to reduce the band gap of TiO_2 by surface modification should have a bulk band gap of less than 5 eV. For example, in the present case, the Ga_2O_3 band gap is around 4.8 eV,[63] while that of MgO is 7.8 eV.[64] We also found that HfO_2 and ZrO_2 modified TiO_2, with bulk band gaps over 5 eV, show no band gap reduction,[45] but other transition metal oxides, such as MoO_2 and Cr_2O_3, band gaps smaller than 5 eV, will reduce the band gap over unmodified TiO_2.[45] Thus, we propose the band gap of the metal oxide that will be deposited on TiO_2 as a useful initial descriptor for reducing the band gap of TiO_2.

3.3. Modelling Charge Separation upon Photoexcitation. Besides the energy gap of a photocatalyst, the fate of the charge carriers produced by light excitation is of paramount importance for photocatalytic activity. The electrons and holes produced upon light excitation must not recombine (which leads to production of only waste heat) so that chemical reactions can take place. This means that the photocatalyst electronic structure must promote charge separation. For doped TiO_2, this is a drawback, as the electronic states induced by doping will promote charge carrier recombination.

To investigate this important point for the present heterostructures, we cannot directly study the excited electronic structure, but instead we use a model for the excited state. This involves a calculation of a triplet state, which by construction must have an unpaired electron and an unpaired hole and appears to be a useful model system to study photoexcited bulk TiO_2[51,52] and has recently been applied in bulk HfO_2.[65]

For TiO_2, Di Valentin and Selloni[51] and Jedidi et al.[52] have shown that this model produces a localised Ti^{3+} electronic state in bulk anatase and the (101) surface[51] and in rutile (110)[52] (from hybrid DFT and DFT+U); a localised oxygen hole state was also found with hybrid DFT.[51] In both studies, singlet-triplet excitation energies have been calculated and relaxation (trapping) energies are presented in ref 51.

For calculations of this model on the present heterostructures, we continue to employ DFT+*U*, with the *U* correction applied to the Ti 3d states. We also apply DFT+*U* to the O 2p states. This correction is necessary since the hole formed upon excitation is localised on an oxygen atom,[51] and many studies have shown that without a +*U* correction or inclusion of exact exchange, localized oxygen hole states are incorrectly described with DFT.[66−69] We use $U = 5.5$ eV on the O 2p states, a value determined by Morgan and Watson for bulk TiO_2[69] using the Koopman's condition of Lany.[70] We first use these values for a calculation on the bare rutile TiO_2 (110) surface and find that the relaxed triplet state has one bridging oxygen carrying the hole and a subsurface Ti^{3+} carrying the electron, consistent with the hybrid DFT results on anatase[51] and consistent with ref 52. for the Ti^{3+} localisation in rutile (110).

With this computational set-up, the following energies are calculated, with reference to the configuration coordinate diagram in Figure 5 that sketches the energies involved:

(1) The singlet-triplet excitation energy: $E^{excite} = E^{singlet} - E^{triplet}$, where both the singlet and triplet electronic states are fully relaxed.

dx.doi.org/10.1021/am301516c | ACS Appl. Mater. Interfaces 2012, 4, 5863−5871

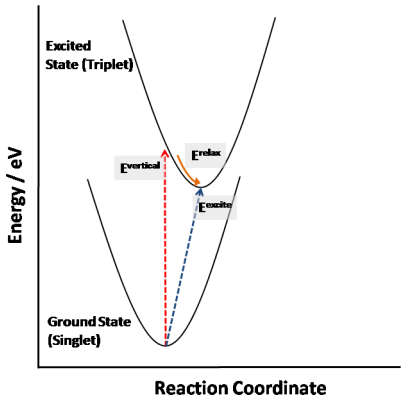

Figure 5. Configuration coordinate diagram indicating the excitation energy, E^{excite}, the vertical transition energy, $E^{vertical}$, and the relaxation energy, E^{relax}, discussed in the text.

(2) The triplet relaxation (or trapping) energy: $E^{relax} = E^{triplet} - E^{triplet@singlet}$, where the first energy is the fully relaxed triplet and the second energy is the triplet state at the singlet geometry (single point calculation), so that E^{relax} is the energy gained when the electron and hole are trapped at their Ti and O sites upon structural relaxation; the importance of the coupling between charge localisation and structural relaxation in systems with localised electronic states is well-known. The vertical excitation energy, $E^{vertical}$, is the energy difference between the singlet ground state and the triplet electronic state at the singlet ground state geometry and is simply given by $E^{excite} + E^{relax}$; $E^{vertical}$ corresponds closely to the simple valence-conduction band energy gap. In contrast to ref 46, we cannot calculate individual electron and hole trapping energies, because we use a three-dimensional periodic slab model.

The excitation and relaxation energies for Ga_2O_3 and MgO-modified TiO_2, along with the bare rutile (110) surface, are shown in table 2. In ref 52., an excitation energy of 1 eV was computed with GGA+U for rutile (110), but the calculation in ref 52., is with a value of U for Ti3d states that is 8 eV (which results in the Ti^{3+} electronic state being in the O2 p valence band, which is not correct) and no correction on the O 2p states. Nonetheless, similar to refs 51. and 52, the excitation energy is smaller than the simple valence-conduction band energy gap (here, 2.1 eV for bare (110) rutile). Unfortunately, no relaxation energies for rutile (110) surface have been published.

Table 2. Excitation and Relaxation Energies for the Triplet Excited State in $(Ga_2O_3)_2$- and $(MgO)_4$-Modified TiO_2 in eV, and the Same Energies for the Bare Rutile (110) Surface

structure	E^{excite} (eV)	E^{relax} (eV)
$(Ga_2O_3)_2$–TiO_2	0.79	1.20
$(MgO)_4$–TiO_2	0.83	1.83
rutile TiO_2 (110)	1.69	0.52

Turning now to the heterostructures, the modification of rutile (110) with Ga_2O_3 and MgO gives a smaller excitation energy and a notably larger relaxation energy. Again, the excitation energy is smaller than the simple band gap calculation and is smaller for both heterostructures compared with the bare TiO_2 surface. This indicates that the excitation energy of MgO- and Ga_2O_3-modified TiO_2 will be reduced over pure TiO_2, which will change the light absorption characteristics. It is possible that in determining the effect of surface modification on the excitation energy, the valence-conduction band energy gap of the ground state, which we have used in section 3.2 to examine the effect of surface modification of TiO_2, may not be sufficient, as analysis of the ground state energy gap leads us to predict that MgO modification will lead to little change in the band gap.

The relaxation energies for both heterostructures are quite large in comparison with the bare TiO_2 rutile (110) surface, which indicates that there is a strong energy gain when the electron and hole are localised and trapped at their lattice sites. We are not able to calculate the individual electron and hole relaxation energies, as outlined at the start of the section, but ref 51. indicates that the hole relaxation energy is notably larger than the electron relaxation energy.

To examine this in more detail, Figure 6 shows the spin density associated with the relaxed triplet state for $(Ga_2O_3)_2$–TiO_2 and $(MgO)_4$–TiO_2. Because this is a triplet electronic state, the spin density indicates the position of the electron and the hole. In both structures, the spin density shows that there is a localised electron on a surface Ti^{3+} site, with a computed Bader charge[71] of +1.7 electrons and a spin magnetisation of 0.90 electrons, both consistent with a Ti^{3+} electronic state. The Ti^{4+} cations have a computed Bader charge of +1.27 electrons. The Ti^{3+} site is found on a subsurface Ti ion, which agrees with the most stable Ti^{3+} site found in refs.[72−74] The hole state is predominantly localised on an oxygen site on the supported nanocluster, with this oxygen having a computed Bader charge of −7.09 electrons (MgO) and −7.07 electrons (Ga_2O_3) and a spin magnetisation of 0.75 electrons (MgO) and 0.70 electrons (Ga_2O_3). Relative to the number of valence electrons, this gives an localised O^- hole (net charge = −1.09 and −-1.07 for oxygen in MgO and Ga_2O_3), for which the Bader charge and magnetisation are typical.[65−69] In contrast, an O^{2-} species has a computed Bader charge of 7.7 electrons.

In particular, the oxygen hole is found on a terminal or low-coordinated cluster oxygen site; that is a singly coordinated oxygen in the MgO cluster and a two coordinated oxygen in Ga_2O_3 and such oxygen sites should be favorable for polaronic hole trapping,[33,51,52] e.g., two-fold surface oxygen on anatase (101)[51] and rutile (110), as mentioned above. The geometry around the oxygen hole site is also shown in Figure 6. The oxygen polaron site in both structures shows the effect of hole localisation. For MgO-TiO_2, the Ti−O distances are 2.00 and 1.93 Å, whereas in Ga_2O_3, the single Ti−O distance is 1.98 Å. In both cases, this bond shows an elongation of ca. 0.2 Å from the Ti−O distance in the singlet ground state. This significant change in the geometry around the hole site would be responsible for the large relaxation energies, as the cluster structure allows larger freedom for the geometry to relax in response to the formation of the localised oxygen hole, which leads to a larger energy gain. Indeed, on the anatase (101) surface, the hole relaxation energy is double that of bulk.[46]

The geometry around the Ti^{3+} sites is also shown in Figure 6. These Ti−O distances are very similar in both structures and are elongated by between 0.1 and 0.12 Å relative to the singlet ground state, which is a smaller change than found for the oxygen hole polaron and would lead to a correspondingly smaller relaxation energy. The lengthening of the distances around the two polaron sites is typical for these states in defective or doped metal oxides.[65−69,72−74]

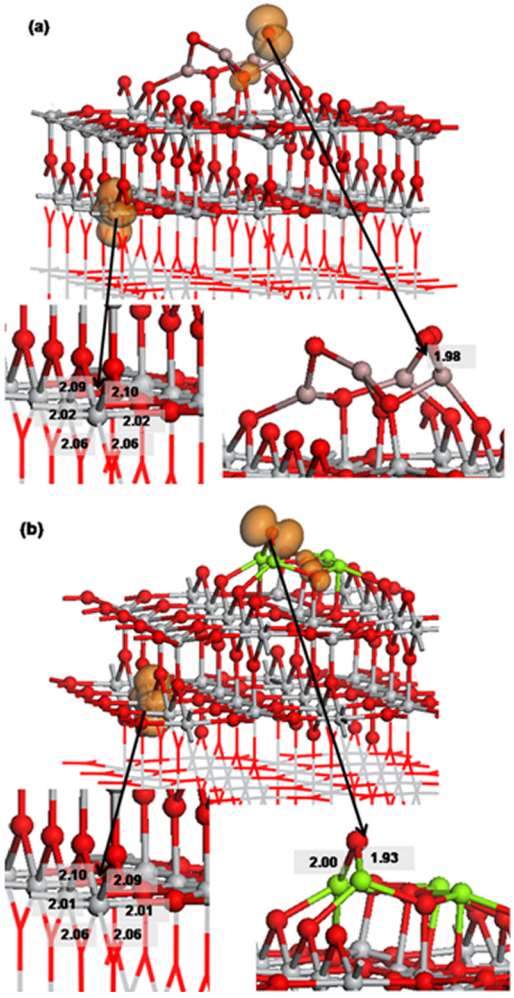

Figure 6. Excess spin density (orange isosurfaces, enclosing spin density values up to 0.02 electrons/Å^3) and metal−oxygen distances (in Å) for Ti^{3+} and O^- polarons in the relaxed triplet excited states of (a) $(Ga_2O_3)_2$ and (b) $(MgO)_4$ adsorbed at the rutile TiO_2 (110) surface.

The crucial finding here is that, as anticipated from the discussion of the electronic properties, our calculations confirm that upon light excitation the electron and hole formed are separated onto the cluster and the surface, in contrast to anatase, where ref 51 shows that the electron and hole are close, which promotes charge recombination. This spatial separation of charge carriers will reduce charge recombination (analysed by photoluminescence spectroscopy[38−42]), thus improving photocatalytic activity and makes the present heterostructures appealing systems as new photocatalysts.

The presence of reduced Ti^{3+} and an oxygen hole is further confirmed in the PEDOS, projected onto Ti 3d states in the surface and O 2p states in the clusters, which is shown in Figure 7. There are two states in the band gap. The first arises from an occupied Ti^{3+} state at around 0.9 eV (Ga_2O_3−TiO_2) and 1 eV (MgO-TiO_2) above the valence band edge. The second state is the empty O 2p state associated with the oxygen hole polaron, which lies 1.5 eV (Ga_2O_3−TiO_2) and 1.8 eV (MgO-TiO_2) above the valence band. Although the precise position of these states in the band gap will depend on the material systems involved, it is important to observe that both heterostructures display the formation of localized polaronic Ti^{3+} and O^- states in the TiO_2 band gap.

These results clearly show that after light excitation the electron and hole produced will be localized on the TiO_2 and on

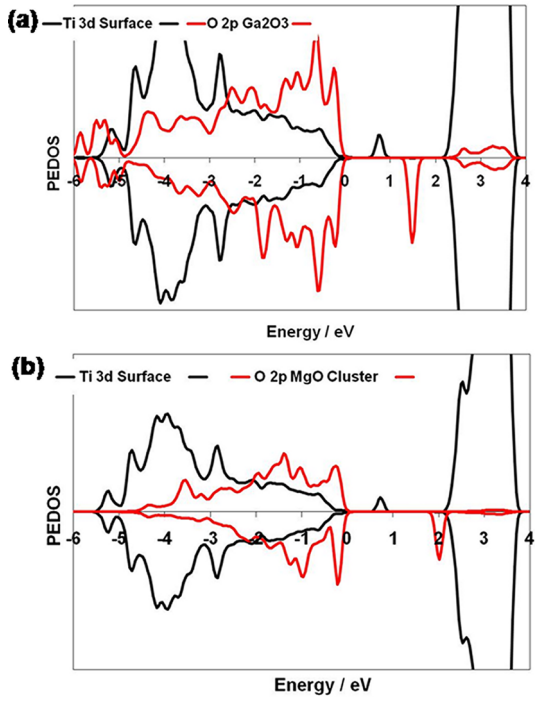

Figure 7. Ti 3d and O 2p PEDOS from the $(Ga_2O_3)_2$ and $(MgO)_4$ clusters for the relaxed triplet excited states for (a) Ga_2O_3-modified TiO_2 and (b) MgO-modified TiO_2. The zero of energy is the top of the valence band.

the metal oxide nanocluster, confirming the suggestions from experiment that this type of heterostructure can promote charge carrier separation, with the consequence that charge recombination will be reduced and photocatalytic activity will be enhanced. Experimental verification of this first-principles prediction will lend support to this model.

4. CONCLUSIONS

From first-principles DFT simulations, we predict that heterostructures composed of rutile TiO_2 (110) modified with Ga_2O_3 and MgO nanoclusters will be photocatalysts with improved photocatalytic activity over pure TiO_2. In particular, Ga_2O_3 modified TiO_2 results in a reduced band gap, into the visible region, and enhanced charge carrier separation after light excitation, which reduces carrier recombination. MgO-modified TiO_2 is predicted to be UV active, but with improved activity.

Both nanoclusters adsorb strongly at the TiO_2 surface, creating new interfacial bonds, which leads to the appearance of new nanocluster derived electronic states around the valence and conduction band edges.

For charge separation, a model of the excited system shows that localised electron and hole polarons are found on surface Ti and oxygen from the cluster, with strong relaxations, thus confirming that charge carrier separation will occur. We propose Ga_2O_3- and MgO-modified rutile TiO_2 as new photocatalysts with improved activity over TiO_2.

AUTHOR INFORMATION

Corresponding Author

*E-mail: michael.nolan@tyndall.ie.

Notes

The authors declare no competing financial interest.

■ ACKNOWLEDGMENTS

This work was supported by Science Foundation Ireland through the Starting Investigator Grant Program (EMOIN SFI SIRG/09/I1620). We also acknowledge SFI-funded computational resources at Tyndall and the SFI/Higher Education Authority funded Irish Centre for High Performance Computing for the generous provision of computing resources.

■ REFERENCES

(1) Ni, M.; Leung, M.; Leung, D.; Sumathy, K. *Renew. Sust. Energy Rev.* **2007**, *11*, 401.
(2) Fujishima, A.; Zhang, X.; Tryk, D. A. *Surf. Sci. Rep.* **2008**, *63*, 515.
(3) Nowotny, J. *Energy Environ. Sci.* **2008**, *2*, 656.
(4) Roy, S.; Varghese, O. K.; Paulose, M.; Grimes, C. A. *ACS Nano* **2010**, *4*, 1259.
(5) Jiang, Z.; Xiao, T.; Kuznetsov, V. L.; Edwards, P. P. *Philos. Trans. R. Soc London, Ser. A.* **2010**, *368*, 3343.
(6) Yu, H.; Irie, H.; Shimodaira, Y.; Hosogi, Y.; Kuroda, Y.; Miyauchi, M.; Hashimoto, K. *J. Phys. Chem. C* **2010**, *114*, 16481.
(7) Murakami, N.; Chiyoya, T.; Tsubota, T.; Ohno, T. *Appl. Catal. A* **2008**, *348*, 148.
(8) Kubacka, A.; Fernandez-Garcia, M.; Colon, G. *Chem. Rev.* **2012**, *112*, 1555.
(9) Di Valentin, C.; Pacchioni, G.; Onishi, H.; Kudo, H. *Chem. Phys. Lett.* **2009**, *469*, 166.
(10) Di Valentin, C.; Finazzi, E.; Pacchioni, G.; Selloni, A.; Livarghi, S.; Paganini, M. C.; Giamello, E. *Chem. Phys* **2007**, *339*, 44.
(11) Yu, J. G.; Xiang, Q. J.; Zhou, M. H.; Zhou, X. Y. *Appl. Catal., B* **2009**, *90*, 595.
(12) R. Long, R.; English, N. J. *J. Phys. Chem. C* **2010**, *114*, 11984.
(13) Zheng, J. W.; Bhattcahrayya, A.; Wu, P.; Chen, Z.; Highfield, J.; Dong, Z. L.; Xu, R. *J. Phys. Chem. C* **2010**, *114*, 7063.
(14) Nie, X. L.; Zhou, S. P.; Maeng, G.; Sohlberg, K. *Int. J. Photoenergy* **2009**, No. 294042.
(15) Cui, Y.; Du, H. H.; Wen, L. S. *J. Mater. Sci. Technol.* **2008**, *24*, 675.
(16) Peng, H. W.; Li, J. B.; Li, S. S.; Xia, J. B. *J. Phys.: Condens. Matter* **2008**, *20*, 125207.
(17) Iwaszuk, A.; Nolan, M. *J. Phys. Chem. C* **2011**, *115*, 12995.
(18) Gai, Y. Q.; Li, J. B.; Li, S. S.; Xia, J. B.; Wei, S. H. *Phys. Rev. Lett.* **2009**, *102*, 036402.
(19) Zhu, W. G.; Qiu, X. F.; Iancu, V.; Chen, X. Q.; Pan, H.; Wang, W.; Dimitrijevic, N. M.; Rajh, T.; Meyer, H. M.; Paranthaman, M. P.; Stocks, G.; Weitering, H. H.; Gu, B. H.; Eres, G.; Zhang, Z. Y. *Phys. Rev. Lett.* **2009**, *103*, 2264101.
(20) Zhang, J.; Pan, C. X.; Fang, P. F.; Wie, J. H.; Xiong, R. *ACS Appl. Mater. Interfaces* **2010**, *2*, 1173.
(21) Yang, H. G.; Sun, C. H.; Qiao, S. Z.; Zou, J.; Liu, G.; Smith, S. C.; Cheng, H. M.; Lu, G. Q. *Nature* **2008**, *453*, 638.
(22) Liu, M.; Piao, L.; Zhao, L.; Ju, S.; Yan, Z.; He, T.; Zhou, C.; Wang, W. *Chem. Commun.* **2010**, *46*, 1664.
(23) Yang, W.; Li, J.; Wang, Y.; Zhu, F.; Shi, W.; Wan, F.; Xu, D. *Chem. Commun.* **2011**, *47*, 1809.
(24) Gu, L.; Wang, J.; Cheng, H.; Du, Y.; Han, X. *Chem. Commun.* **2012**, *48*, 6978.
(25) Dai, Y. Q.; Cobley, C. M.; Zeng, J.; Sun, Y. M.; Xia, Y. N. *Nano Lett.* **2009**, *9*, 2455.
(26) Qiu, J.; Zhang, S.; Zhao, H. *J. Hazard. Mater.* **2012**, *211-212*, 381.
(27) Aprile, C.; Corma, A.; Garcia, H. *Phys. Chem. Chem. Phys.* **2008**, *10*, 769.
(28) Kronawitter, C. X.; Vayssieres, L.; Shen, S.; Guo, L.; Wheeler, D. A.; Zhang, J. Z.; Antoun, B. R.; Mao, S. S. *Energy Environ. Sci.* **2011**, *4*, 3889.
(29) Frame, F. A.; Townsend, T. K.; Chamousis, R. L.; Sabio, E. M.; Dittrich, Th.; Browning, N. D.; Osterloh, F. E. *J. Am. Chem. Soc.* **2011**, *133*, 7264.
(30) Law, M.; Greene, L. E.; Johnson, J. C.; Saykally, R.; Yang, P. *Nat. Mater.* **2005**, *4*, 455.
(31) Y. Cao, Y.; He, T.; Chen, Y.; Cao, Y. *J. Phys. Chem. C* **2010**, *114*, 3627.
(32) Kong, L.; Jiang, Z.; Xiao, T.; Lu, L.; Jones, M.; Edwards, P. P. *Chem. Commun.* **2011**, *47*, 5512.
(33) Cheng, H.; Huang, B.; Dai, Y.; Qin, X.; Zhang, X. *Langmuir* **2010**, *26*, 6618.
(34) Hong, S.; Lee, S.; Jang, J.; Lee, J. *Energy Environ. Sci.* **2011**, *4*, 1781.
(35) Cao, T.; Li, Y.; Wang, C.; Zhang, Z.; Zhang, M.; Shao, C.; Liu, Y. *J. Mater. Chem.* **2011**, *21*, 6922.
(36) V. Bharat, V.; Boppana, R.; Lobo, R. F. *ACS Catal.* **2011**, *1*, 923.
(37) J. Libera, J.; Elam, J.; Sather, N.; Rajh, T.; Dimitrijevic, N. M. *Chem. Mater.* **2010**, *22*, 409.
(38) H. Tada, H.; Jin, Q.; Nishijima, H.; Yamamoto, H.; Fujishima, M.; Okuoka, S-i.; Hattori, T.; Sumida, Y.; Kobayashi, H. *Angew Chem., Int. Ed.* **2011**, *50*, 3501.
(39) Jin, Q.; Fujishima, M.; Tada, H. *J. Phys. Chem C* **2011**, *115*, 6478.
(40) Q. Jin, Q.; Ikeda, Y.; Fujishima, M.; Tada, H. *Chem. Commun.* **2011**, *47*, 8814.
(41) M. Fujishima, M.; Jin, Q.; Yamamoto, H.; Tada, H.; Nolan, M. *Phys. Chem. Chem. Phys.* **2012**, *14*, 705.
(42) Jin, Q.; Fujishima, M.; Nolan, M.; Iwaszuk, A.; Tada, H. *J. Phys. Chem. C* **2012**, *116*, 12621.
(43) Nolan, M. *Phys. Chem. Chem. Phys.* **2011**, *13*, 18194.
(44) Iwaszuk, A.; Nolan, M. *Phys. Chem. Chem. Phys.* **2011**, *13*, 4963.
(45) Nolan, M. *Chem. Commun* **2011**, *47*, 8617.
(46) Shao, Z.; Tian, B.; Zhang, J. *Mater. Lett.* **2009**, *63*, 1705.
(47) Bandara, J.; Kuruppu, S. S.; Pradeep, U. W. *Colloids Surf., A* **2006**, *276*, 197.
(48) Bandara, J.; Hadapangoda, C. C.; Jayasekera, W., G. *Appl. Catal., B* **2004**, *50*, 83.
(49) Jung, H. S.; Lee, J.-K.; Nastasi, M.; Kim, J.-R.; Lee, S. W.; Kim, J. Y.; Park, J. S.; Hong, K. S.; Shin, H. *Appl. Phys. Lett.* **2006**, *88*, 0103107.
(50) Tada, H.; Yamamoto, M.; Ito, S. *J. Electrochem Soc.* **2000**, *147*, 613.
(51) Di Valentin, C.; Selloni, A. *J. Phys. Chem. Lett.* **2011**, *2*, 222.
(52) Jedidi, A.; Markovits, A.; Minot, C.; Bouzriba, S.; Abderraba, M. *Langmuir* **2010**, *26*, 16232.
(53) Kresse, G.; Hafner, J. *Phys. Rev. B* **1994**, *49*, 1425.
(54) Blöchl, P. E. *Phys. Rev. B* **1994**, *50*, 17953.
(55) J. P. Perdew In *Electronic Structure of Solids '91*; Ziesche, P., Eschrig, H., Eds.; Akademie Verlag: Berlin, 1991.
(56) Anisimov, V. I.; Zaanen, J.; Andersen, O. K. *Phys. Rev. B* **1991**, *44*, 943.
(57) Dudarev, S. L.; Botton, G. A.; Savrasov, S. Y.; Humphreys, C. J.; Sutton, A. P. *Phys. Rev. B* **1998**, *57*, 1505.
(58) Morgan, B. J.; Watson, G. W. *Surf. Sci.* **2007**, *601*, 5034.
(59) Mulheran, P. A.; Nolan, M.; Browne, C. S.; Basham, M.; Sanville, E.; Bennett, R. A. *Phys. Chem. Chem. Phys.* **2010**, *12*, 9763.
(60) Graciani, J.; Plata, J. J.; Fdez Sanz, J.; Liu, P.; Rodriguez, J. A. *J. Chem. Phys* **2010**, *132*, 104703.
(61) Haertelt, M.; Fielicke, A.; Meijer, G.; Kwapien, K.; Sierka, M.; Sauer, J. *Phys. Chem. Chem. Phys.* **2012**, *14*, 2849.
(62) Rahane, A. B.; Deshpande, M. D. *J. Phys. Chem. C* **2012**, *116*, 2691.
(63) Yamaga, M.; Ishikawa, T.; Yoshida, M.; Hasegawa, T.; Villora, E. G.; Shimamura, K. *Phys. Status Solidi C* **2011**, *8*, 2621.
(64) Taurian, O. E.; Springborg, M.; Christensen, N. E. *Solid State Commun.* **1985**, *55*, 351.
(65) McKenna, K. P.; Wolf, M. J.; Shluger, A. L.; Lany, S.; Zunger, A. *Phys. Rev. Lett.* **2012**, *108*, 116403.
(66) Nolan, M.; Watson, G. W. *J. Chem. Phys.* **2006**, *125*, 144701.
(67) Scanlon, D. O.; Walsh, A.; Morgan, B. J.; Fearon, J. E.; Nolan, M.; Watson, G. W. *J. Phys. Chem. C* **2007**, *111*, 7971.
(68) Keating, P. R. L.; Scanlon, D. O.; Morgan, B. J.; Galea, N. M.; Watson, G. W. *J. Phys. Chem. C* **2012**, *116*, 2443.
(69) Morgan, B. J.; Watson, G. W. *J. Phys. Chem. C* **2010**, *114*, 2321.
(70) Lany, S.; Zunger, A. *Phys. Rev. B* **2011**, *80*, 085202.

(71) Henkelman, G.; Arnaldsson, A.; Jónsson, H. *Comput. Mater. Sci.* **2006**, *36*, 25.
(72) Kowalski, P. M.; Camellone, M. F.; Nair, N. N.; Meyer, B.; Marx, D. *Phys. Rev. Lett.* **2010**, *105*, 146405.
(73) Deskins, N. A.; Rousseau, R.; Dupuis, M. *J. Phys. Chem. C* **2011**, *115*, 7562.
(74) Chretien, S.; Metiu, H. *J. Phys. Chem. C* **2011**, *115*, 4705.